High Step-Up DC-DC Converter with Switched Multi-inductor Technique

Lung-Sheng Yang and Jing-Han Cai
Department of Electrical Engineering, Far East University, Tainan City, Taiwan
Email: yanglungsheng@yahoo.com.tw, ciselsky@gmail.com

***Abstract*—This paper presents a single-switch high step-up DC-DC converter. The pulse-width modulation is used to control the switch. The switched multi-inductor technique is adopted for achieving high step-up voltage gain. Three inductors with same level of inductance are employed for the proposed converter. When the switch is turned on, these three inductors store their energies by parallel connection. While the switch is turned off, the energies stored in the three inductors are released by serial connection. The switched-inductor technique can be extended to multi-inductor for providing higher voltage gain. In order to show the performance of the proposed converter, a prototype hardware circuit is implemented.**

***Index Terms*—pulse-width modulation, switched inductor, high step-up**

I. Introduction

In the past decades, some literatures are presented the electrical conversion for the renewable energy power supply system [1], [2]. The boost converter is used to provide step-up voltage conversion [3]-[5]. However, the boost converter can't provide enough step-up voltage conversion owing to the impact of the forward-voltage drop of diode, the conducting resistance of switch, and the equivalent series resistance of inductor and capacitor. In order to provide higher step-up voltage conversion, some converters are studied. These converters include the cascaded boost types [6], [7], voltage-lift types [8], [9], switched-capacitor types [10], voltage-quadrupler types [11], [12], and switched-inductor types [12], [13]. The switched-inductor types employ the parallel-charge and series-discharge technique to obtain high voltage gain. The 2-inductor types are used in the converters, as shown in Fig. 1. In order to provide higher voltage gain, the high step-up DC-DC converter with switched 3-inductor technique is investigated in this paper. The circuit structure of the proposed converter is shown in Fig. 2. Only a single switch is used in the proposed converter. The switched-inductor technique adopts three inductors with same level of inductance. The 3-inductor type is charged by parallel during the switch ON-period and is discharged by series during the switch OFF-period.

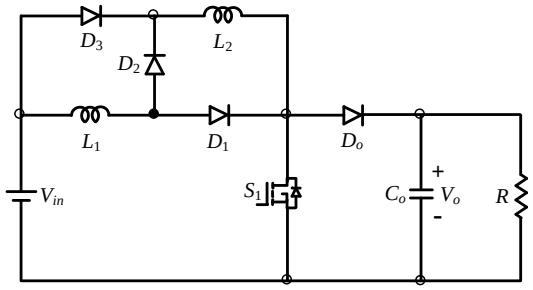

Figure 1. Switched 2-inductor high step-up converter.

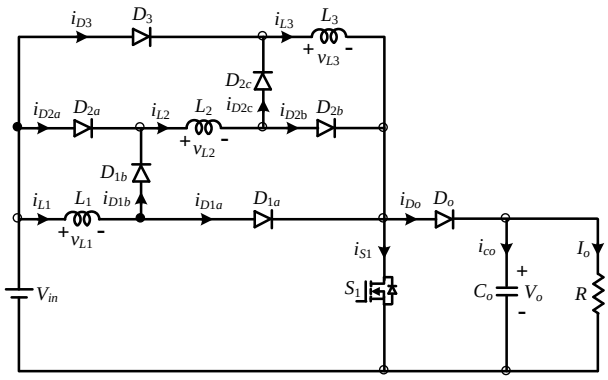

Figure 2. Circuit structure of the proposed converter.

II. Operating Principles

One utilizes the pulse-width-modulation technique to control the switch S_1. The three inductors L_1, L_2, and L_3 have same inductance, namely $L_1 = L_2 = L_3 = L$.

A. Continuous Conduction Mode (CCM) Operation

Fig. 3 shows some key waveforms in CCM operation. The operating principles of the proposed converter are explained as follows:

(1) Mode 1, [t_0, t_1]: The switch S_1 is turned on. The current flow is shown in Fig. 4(a). The source V_{in} transfers its energy to the three inductors L_1, L_2, and L_3. Meanwhile, the three inductors L_1, L_2, and L_3 are charged in parallel connection. Therefore, the three inductor-current i_{L1}, i_{L2}, and i_{L3} are increased linearly, as shown in Fig. 3. The energy of the output capacitor C_o is discharged to the load R.

Manuscript received September 19, 2018; revised May 8, 2019.

doi: 10.18178/ijoee.7.1.15-20

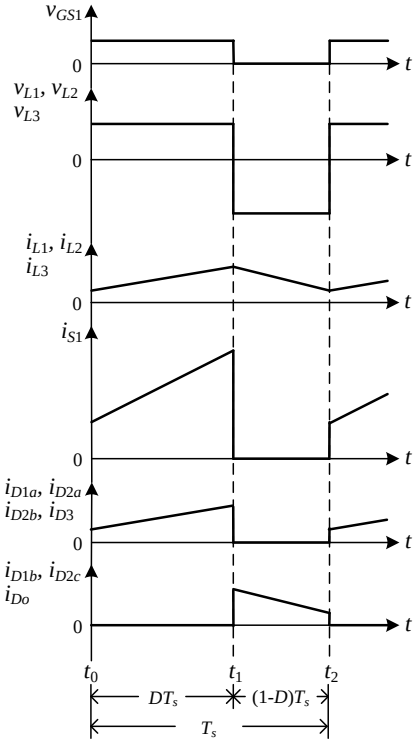

Figure 3. Some key waveforms in CCM operation.

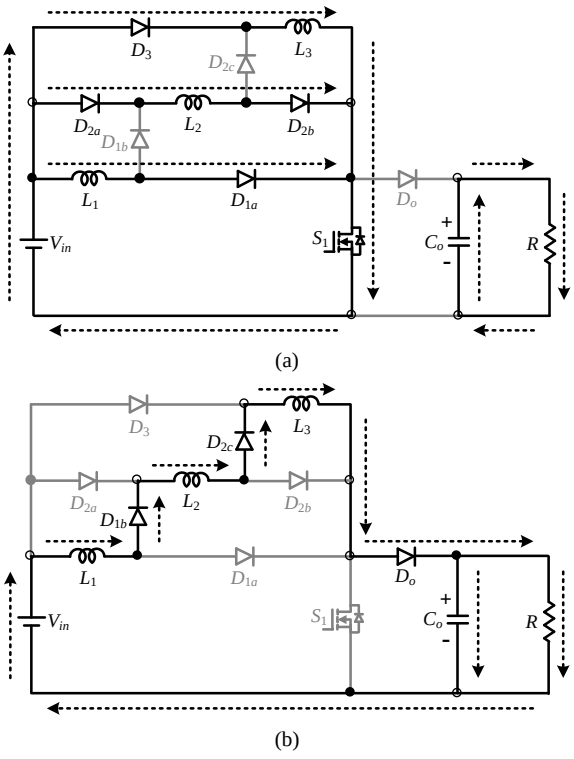

Figure 4. Current flow of the operating modes. (a) Mode 1. (b) Mode 2.

(2) Mode 2, [t_1, t_2]: The switch S_1 is turned off.The current flow is shown in Fig. 4(b). The source V_{in} and the three inductors L_1, L_2, and L_3 release their energies to the output capacitor C_o and load R. Meanwhile, the three inductors L_1, L_2, and L_3 are in series connection. Therefore, the three inductor-current i_{L1}, i_{L2}, and i_{L3} are decreased linearly, as shown in Fig. 3.

B. Discontinuous Conduction Mode (DCM) Operation

Fig. 5 shows some key waveforms in DCM operation. The operating principle is explained as follows:

(1) Mode 1, [t_0, t_1]: The switch S_1 is turned on. The current flow is shown in Fig. 4(a). The operating principle is the same as the mode 1 of CCM operation.

(2) Mode 2, [t_1, t_2]: The switch S_1 is turned off. The current flow is shown in Fig. 4(b). The operating principle is the same as the mode 2 of CCM operation.

(3) Mode 3, [t_2, t_3]: The switch S_1 is still turned off. The current flow is shown in Fig. 6. The energies stored in the three inductors L_1, L_2, and L_3 are released to empty at $t = t_2$. It can be seen from Fig. 5 that the three inductor-current i_{L1}, i_{L2}, and i_{L3} are zero. The energy stored in the output capacitor C_o is discharged to the load R.

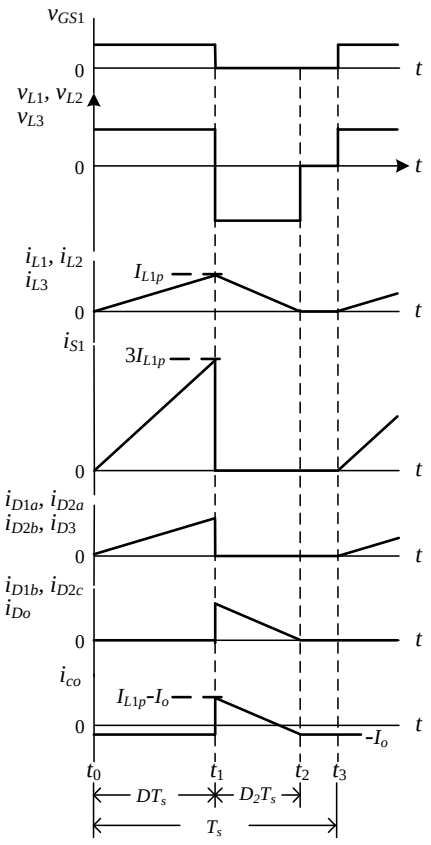

Figure 5. Some key waveforms in DCM operation.

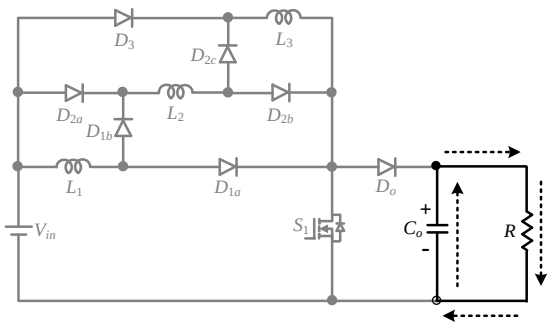

Figure 6. Current direction for the mode 3 of DCM operation.

III. Steady-State Analysis

A. CCM Operation

When the proposed converter is operated in the mode 1, the voltages across the three inductors L_1, L_2, and L_3 are written as follows.

$$v_{L1} = v_{L2} = v_{L3} = V_{in} \tag{1}$$

Owing to $L_1 = L_2 = L_3 = L$, the differential equation of the three inductor-current are obtained as

$$\frac{di_{L1}(t)}{dt} = \frac{di_{L2}(t)}{dt} = \frac{di_{L3}(t)}{dt} = \frac{V_{in}}{L} \tag{2}$$

Thus, one can derive the three inductor-current as

$$i_{L1} = i_{L2} = i_{L3} = \frac{V_{in}}{L}(t - t_0) + i_{L1}(t_0), \quad t_0 \le t \le t_1 \tag{3}$$

When the proposed converter is operated in the mode 2, the voltages across the three inductors L_1, L_2, and L_3 are given as

$$v_{L1} + v_{L2} + v_{L3} = V_{in} - V_o \tag{4}$$

Therefore,

$$v_{L1} = v_{L2} = v_{L3} = \frac{V_{in} - V_o}{3} \tag{5}$$

Then, the differential equation of the three inductor-current are written as follows.

$$\frac{di_{L1}(t)}{dt} = \frac{di_{L2}(t)}{dt} = \frac{di_{L3}(t)}{dt} = \frac{V_{in} - V_o}{3L} \tag{6}$$

Thus, the three inductor-current are found as

$$i_{L1} = i_{L2} = i_{L3} = \frac{V_{in} - V_o}{3L}(t - t_1) + i_{L1}(t_1), \quad t_1 \le t \le t_2 \tag{7}$$

According to the volt-second balance principle on the inductor L_1, the following equation is written as

$$\int_0^{t_1} v_{L1} dt + \int_{t_1}^{t_2} v_{L1} dt = 0 \tag{8}$$

Substituting (1) and (5) into (8), one obtains the following equation.

$$V_{in} D + \frac{V_{in} - V_o}{3}(1 - D) = 0 \tag{9}$$

The voltage gain of the proposed converter in CCM operation can be found as follows.

$$M_{CCM} = \frac{V_o}{V_{in}} = \frac{1 + 2D}{1 - D} \tag{10}$$

The curves of the voltage gain in CCM operation is displayed in Fig. 7. It can be seen that the proposed converter can be applied for high step-up voltage gain applications.

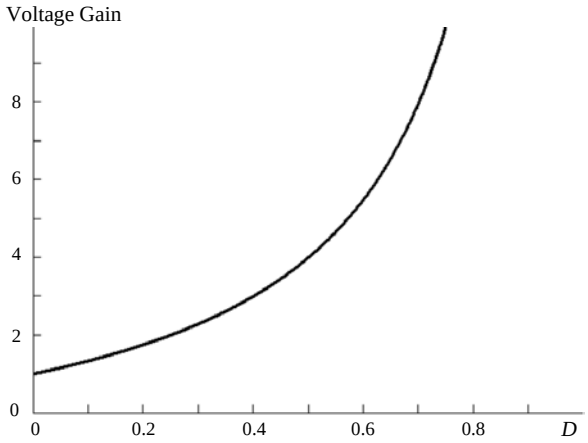

Figure 7. Voltage gain of in CCM operation.

B. DCM Operation

When the proposed converter is operated in the mode 1, the peak values of the three inductor-current i_{L1}, i_{L2}, and i_{L3} are derived from (2) as follows.

$$I_{L1p} = I_{L2p} = I_{L3p} = \frac{V_{in}}{L} D T_s \tag{11}$$

When the proposed converter is operated in the mode 2, the peak values of the three inductor-current i_{L1} and i_{L2} are given from (6) as follows.

$$I_{L1p} = I_{L2p} = I_{L3p} = \frac{V_o - V_{in}}{3L} D_2 T_s \tag{12}$$

Using (11) and (12), one can find the parameter D_2.

$$D_2 = \frac{3DV_{in}}{V_o - V_{in}} \tag{13}$$

From Fig. 5, the average value of the output-capacitor current during each switching period is written as

$$I_{co} = \frac{\frac{I_{L1p} D_2 T_s}{2} - I_o T_s}{T_s} = \frac{I_{L1p} D_2}{2} - I_o \tag{14}$$

Substituting (11) and (13) into (14), the average value of the output-capacitor current is derived as

$$I_{co} = \frac{3D^2 T_s V_{in}^2}{2L(V_o - V_{in})} - \frac{V_o}{R} \tag{15}$$

The average value of the output-capacitor current is equal to zero at steady state. The equation (15) is rewritten as

$$\frac{3D^2 T_s V_{in}^2}{2L(V_o - V_{in})} = \frac{V_o}{R} \tag{16}$$

One defines the inductor time constant as follows.

$$\tau_L \equiv \frac{L}{RT_s} \tag{17}$$

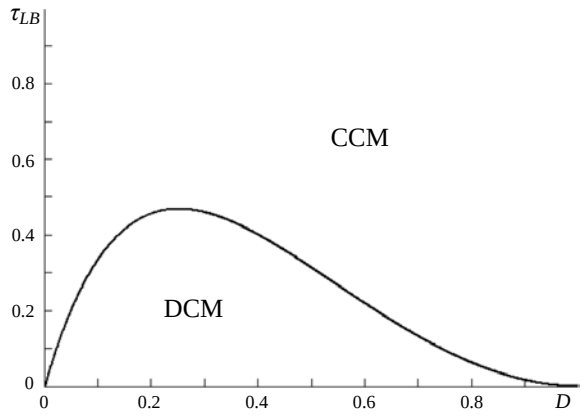

Figure 8. Boundary condition of the proposed converter.

Substituting (17) into (16), the voltage gain in DCM operation is obtain as follows.

$$M_{DCM} = \frac{V_o}{V_{in}} = \frac{1}{2} + \sqrt{\frac{1}{4} + \frac{3D^2}{2\tau_L}} \tag{18}$$

C. Boundary Operating Condition of CCM and DCM

When the proposed converter is operated in boundary conduction mode, the voltage gain in CCM operation equals the voltage gain in DCM operation. Using (10) and (18), the boundary inductor time constant τ_{LB} is found as follows.

$$\tau_{LB} = \frac{D(1-D)^2}{2(1+2D)} \tag{19}$$

Fig. 8 shows the curve of the boundary inductor time constant τ_{LB}. If the inductor time constant τ_L is larger than the boundary inductor time constant τ_{LB}, the proposed converter is operated in CCM.

D. Voltage Stress on the Power Devices

From Fig. 4(a), the voltage stresses on the three diodes D_{1b}, D_{2c}, and D_o are known as follows.

$$V_{D1b} = V_{D2c} = V_{in} \tag{20}$$

$$V_{Do} = V_o \tag{21}$$

From Fig. 4(b), the voltage stresses on the four diodes D_{1a}, D_{2a}, D_{2b}, D_3, and switch S_1 are found as follows.

$$V_{D1a} = V_{D3} = \frac{2(V_o - V_{in})}{3} \tag{22}$$

$$V_{D2a} = V_{D2b} = \frac{V_o - V_{in}}{3} \tag{23}$$

$$V_{S1} = V_o \tag{24}$$

IV. Extension of the Proposed Converter

The 3-inductor type is utilized for the proposed converter to achieve high voltage gain. Of course, the switched-inductor technique can be extended to the 4-inductor and multi-inductor types, as displayed in Fig. 9. According to the volt-second balance principle on the inductor L_1, the voltage gains of the 4-inductor and multi-inductor types can be found as follows.

$$M_{CCM\,(4-inductor)} = \frac{V_o}{V_{in}} = \frac{1+3D}{1-D} \tag{25}$$

$$M_{CCM\,(multi-inductor)} = \frac{V_o}{V_{in}} = \frac{1+(n-1)D}{1-D} \tag{26}$$

V. Experimental Results

The prototype circuit is built for verifying the performance. The electric specifications and circuit components are selected as follows.

(1) Input voltage V_{in} = 25 V
(2) Output voltage V_o = 200 V
(3) Output power P_o = 120 W
(4) Switching frequency f_s = 75 kHz
(5) Capacitor C_o = 100 μF
(6) Switch S_1: IXTQ69N30P
(7) Diodes D_{1a}~D_3: DPG30C200PB, D_o: STTH6003CW

The voltage gain M equals 8. Substituting M = 8 into (10), the duty ratio D is given as 0.7. Substituting D = 0.7 into (19), the boundary time constant τ_{LB} is 0.013.

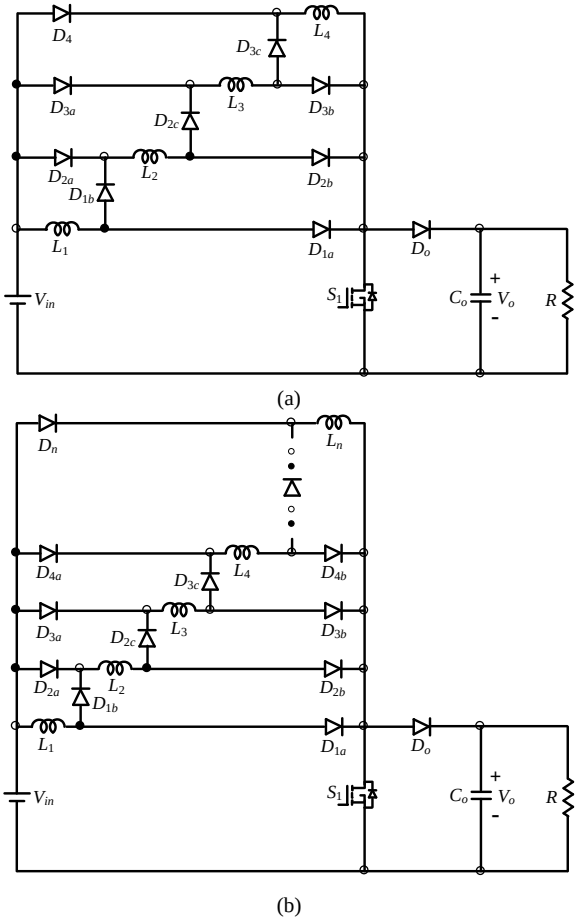

Figure 9. Extended topologies of the switched-inductor type. (a) 4-inductor type. (b) multi-inductor type.

One sets that the proposed converter is operated in CCM from 30% of the full load. Therefore, the load R is 1111 Ω. When the time constant τ_L is larger than the boundary time constant τ_{LB}, the proposed converter is operated in CCM. Hence,

$$L > \frac{R}{f_s}\tau_{LB} = \frac{1111}{75\text{k}} \times 0.013 = 193\ \mu\text{H}$$

Thus, the three inductors L_1, L_2, and L_3 are selected as 196 μH. The experimental results are displayed in Figures 10 and 11. The waveforms of the three inductor-current i_{L1}, i_{L2}, and i_{L3} are shown in Fig. 10(a). It is seen that the proposed converter is operated in CCM and the three inductor-current i_{L1}, i_{L2}, and i_{L3} are almost the same. Fig. 10(b) shows the waveforms of the switch-current i_{S1} and diode-current i_{D1a}. During the switch ON period, the switch-current i_{S1} equals the summation of inductor-current i_{L1}, i_{L2}, i_{L3}. Also, the diode-current i_{D1a} equals the inductor-current i_{L1}. The waveforms of the two diode-current i_{D1b} and i_{Do} are shown in Fig. 10(c). One can see that the diode-current i_{D1b} equals the diode-current i_{Do} during the switch OFF period. Fig. 10(d) shows the waveforms of the switch-voltage v_{S1} and diode-voltage v_{Do}. At steady state, the voltage stresses on the power devices S_1 and D_o equal the output voltage V_o. Fig. 10(e) shows the waveforms of the three diode-voltage v_{D1a}, v_{D1b}, and v_{D2a}. The voltage stresses on the three diodes D_{1a}, D_{1b}, and D_{2a} are approximately 120 V, 25 V, and 60 V respectively. They agree to the theoretical analysis. As shown in Fig. 10(f), the output voltage V_o is controlled in 200 V. Fig. 11 shows the measured efficiency of the proposed converter, it can be seen that the maximum and full-load efficiencies are 92.6% and 92.1% respectively.

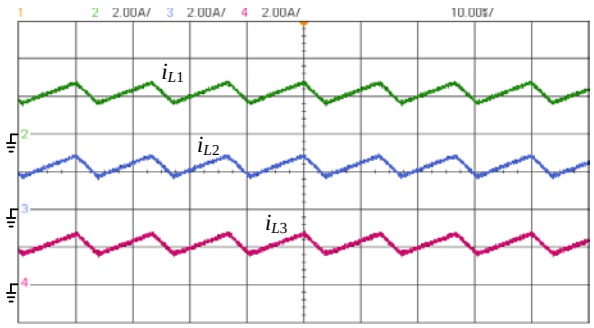

i_{L1}, i_{L2}, i_{L3}: 2 A/div, Time: 10 μs/div

(a)

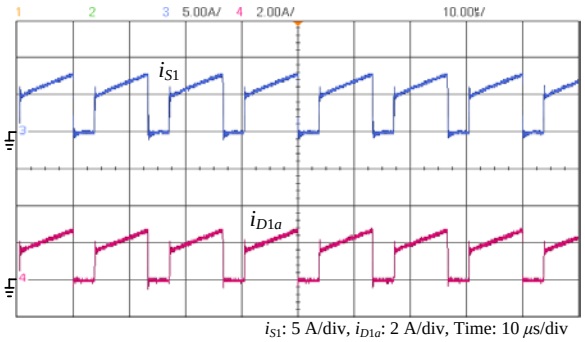

i_{S1}: 5 A/div, i_{D1a}: 2 A/div, Time: 10 μs/div

(b)

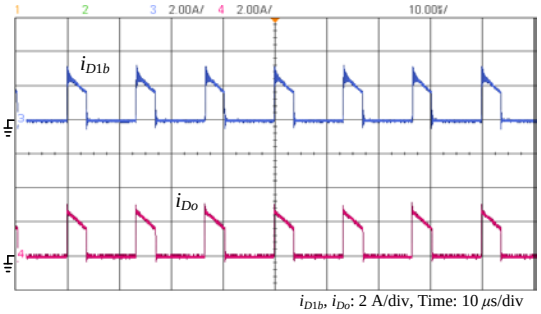

i_{D1b}, i_{Do}: 2 A/div, Time: 10 μs/div

(c)

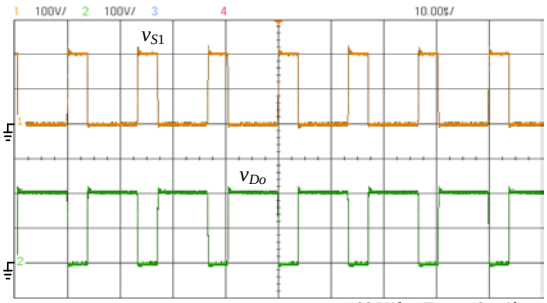

v_{S1}, v_{Do}: 100 V/div, Time: 10 μs/div

(d)

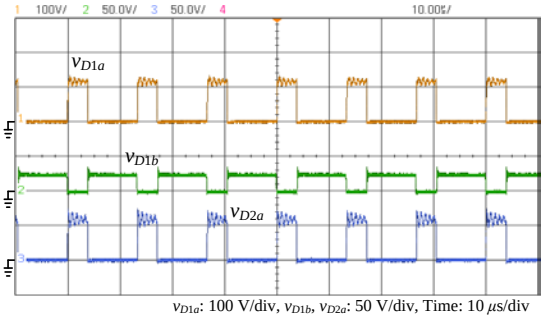

v_{D1a}: 100 V/div, v_{D1b}, v_{D2a}: 50 V/div, Time: 10 μs/div

(e)

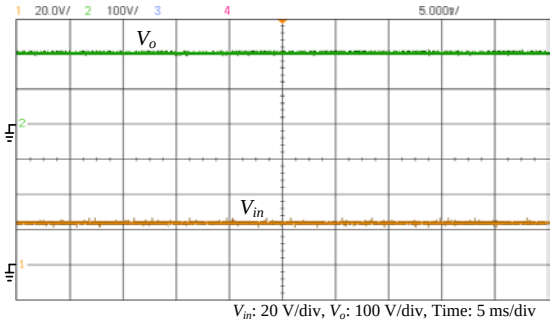

V_{in}: 20 V/div, V_o: 100 V/div, Time: 5 ms/div

(f)

Figure 10. Experimental waveforms. (a) i_{L1}, i_{L2}, and i_{L3}, (b) i_{S1} and i_{D1a}, (c) i_{D1b} and i_{Do}, (d) v_{S1} and v_{Do}, (e) v_{D1a}, v_{D1b}, and v_{D2a}, (f) V_{in} and V_o.

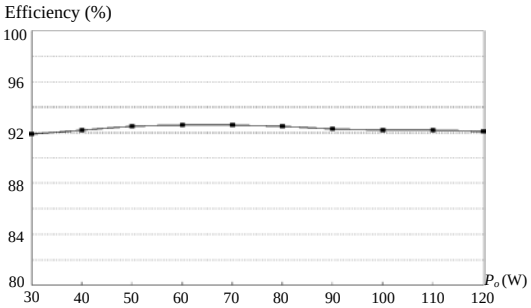

Figure 11. Measured efficiency of the proposed converter.

VI. Conclusions

A high step-up DC-DC converter is investigated in this paper. The switched multi-inductor technique is employed for the proposed converter. For achieving high voltage gain, the parallel-charge and series-discharge method are applied to these inductors. The operating principles in CCM operation and DCM operation are described. The boundary condition is also discussed. From the experimental results, one can see that the high voltage gain is implemented. Also, the experimental waveforms agree with the operating principles and steady-state analyses. The maximum efficiency is 92.6% and the full-load efficiency is 92.1%.

Acknowledgment

The authors gratefully acknowledge financial support from the Ministry of Science and Technology of Taiwan under project MOST 107-2637-E-269-006.

References

[1] M. H. Todorovic, L. Palma, and P. N. Enjeti, "Design of a wide input range DC-DC converter with a robust power control scheme suitable for fuel cell power conversion," *IEEE Trans. Ind. Electron.*, vol. 55, no. 3, pp. 1247-1255, Mar. 2008.

[2] T. V. Thang, N. M. Thao, J. H. Jang, and J. H. Park, "Analysis and design of grid-connected photovoltaic systems with multiple-integrated converters and a pseudo-DC-link inverter," *IEEE Trans. Ind. Electron.*, vol. 61, no. 7, pp. 3377-3386, Jul. 2014.

[3] N. S. Ting, Y. Sahin, and I. Aksoy, "Analysis, design, and implementation of a zero-voltage-transition interleaved boost converter," *Journal of Power Electron.*, vol. 17, no. 1, pp. 41-45, Jan. 2017.

[4] S. Oucheriah and L. Guo, "PWM-based adaptive sliding-mode control for boost DC-DC converters," *IEEE Trans. Ind. Electron.*, vol. 60, no. 8, pp. 3291-3294, Aug. 2013.

[5] M. K. Nguyen, Y. O. Choi, G. B. Cho, and Y. C. Lim, "Two-switch non-isolated step-up DC-DC converter," *Journal of Power Electron.*, vol. 18, no. 3, pp. 651-661, May. 2018.

[6] R. Haroun, A. E. Aroudi, A. C. Pastor, G. Garcia, C. Olalla, and L. M. Salamero, "Impedance matching in photovoltaic systems using cascaded boost converters and sliding-mode control," *IEEE Trans. Power Electron.*, vol. 30, no. 6, pp. 3185-3199, Jun. 2015.

[7] O. L. Santos, L. M. Salamero, G. Garcia, H. V. Blavi, and T. S. Polanco, "Robust sliding-mode control design for a voltage regulated quadratic boost converter," *IEEE Trans. Power Electron.*, vol. 30, no. 4, pp. 2313-2327, Apr. 2015.

[8] F. L. Luo and H. Ye, "Positive output multiple-lift push-pull switched-capacitor Luo-converters," *IEEE Trans. Ind. Electron.*, vol. 51, no. 3, pp. 594-602, Jun. 2004.

[9] Y. Jiao, F. L. Luo, and B. K. Bose, "Voltage-lift split-inductor-type boost converters," *IET Power Electron.*, vol. 4, no. 4, pp. 353-362, 2011.

[10] G. Wu, X. Ruan, and Z. Ye, "Nonisolated high step-up DC-DC converters adopting switched-capacitor cell," *IEEE Trans. Ind. Electron.*, vol. 62, no. 1, pp. 383-393, Jan. 2015.

[11] C. T. Pan, C. F. Chuang, and C. C. Chu, "A novel transformer-less adaptable voltage quadrupler DC converter with low switch voltage stress," *IEEE Trans. Power Electron.*, vol. 29, no. 9, pp. 4787-4796, Sep. 2014.

[12] Y. Tang, T. Wang, and D. Fu, "Multicell switched-inductor/switched-capacitor combined active-network converters," *IEEE Trans. Power Electron.*, vol. 30, no. 4, pp. 2063-2072, Apr. 2015.

[13] Y. Tang, D. Fu, T. Wang, and Z. Xu, "Hybrid switched-inductor converters for high step-up conversion," *IEEE Trans. Ind. Electron.*, vol. 62, no. 3, pp. 1480-1490, Mar. 2015.

Lung-Sheng Yang was born in Taiwan, in 1967. He received his B.S. degree in Electrical Engineering from National Taiwan Institute of Technology, Taiwan, his M.S. degree in Electrical Engineering from National Tsing-Hua University, Taiwan, and his Ph.D degree in Electrical Engineering from National Cheng-Kung University in 1990, 1992, and 2007, respectively. He is currently with the Department of Electrical Engineering, Far East University, Tainan, where he is an Associate Professor. His research interests are power factor correction, dc-dc converters, and renewable energy conversion.

Jing-Han Cai received B.S. degree in Electrical Engineering from Far East University, Tainan City, Taiwan, in 2016. His research interests are power factor correction, and dc-dc converters.